

Conception and Realization of a Wideband Directional Dual-Beam Phased MIMO Array Antenna with Hybrid Coupler for ISM Band Utilizations

Abdelaaziz El Ansari^{1,*}, Shobhit K. Khandare², Najiba El Amrani El Idrissi¹, Abdelhak Bendali¹, Sudipta Das³, Fatima Younis⁴, Hala K. Abduljaleel⁵, and Ahmed Jamal Abdullah Al-Gburi^{6,*}

¹Signal, System and Component Laboratory, Sidi Mohamed Ben Abdellah University — FST Fez, Morocco

²Vivekanand Education Society's Institute of Technology (VESIT), Mumbai, India

³Department of Electronics and Communication Engineering, IMPS College of Engineering and Technology, India

⁴School of Physics, Central South University, Changsha 410083, China

⁵College of Engineering, Al-Iraqia University, Saba'a Abkar Complex, Baghdad, Iraq

⁶Center for Telecommunication Research & Innovation (CeTRI)

Fakulti Teknologi Dan Kejuruteraan Elektronik Dan Komputer (FTKEK)

Jalan Hang Tuah Jaya, 76100, Durian Tunggal, Melaka, Universiti Teknikal Malaysia Melaka (UTeM), Malacca, Malaysia

ABSTRACT: This work addresses a wideband dual-beam 1×4 phased MIMO array antenna with a hybrid coupler for Industrial, Scientific and Medical (ISM) bands applications at 2.4–2.5 GHz. We engineered, refined, and reduced the fundamental component utilizing the novel concept of an advanced curved quarter-wave impedance adapter, achieving a 50% reduction in size relative to comparable designs documented in the literature. The fundamental component operates at 2.45 GHz, including a narrow bandwidth of 26 MHz and a maximum gain of 7.21 dB. Subsequently, a lossless magic-T power splitter is employed to feed two identical miniaturized elements resulting in a compact 1×2 array antenna with miniaturized size and enhanced performance. The obtained results show that the miniaturized 1×2 array antenna resonates at 2.45 GHz with a narrow impedance bandwidth of 52 MHz, peak gain of 9.41 dB, and peak directivity of 9.48 dB at 2.45 GHz. To broaden the narrow bandwidth and enhance gain directivity and radiation coverage area, a 3 dB hybrid coupler is used to feed two identical miniaturized 1×2 array antennas resulting a wideband directional dual-beam MIMO phased 1×4 array antenna. The proposed dual-beam array antenna prototype has been designed and fabricated on a substrate Rogers RT/duroid 5880 with the following parameters: relative permittivity $\epsilon_r = 2.2$, dielectric loss tangent of 0.0009, and total size of $240 \times 136 \times 1.56 \text{ mm}^3$. The simulation results are corroborated by experiments that verified the proposed dual-beam MIMO array antenna which exhibits a high gain of 11.2 dB, effective adaptation, an expanded bandwidth of 1.22 GHz, in addition to its MIMO capability and the dual beams oriented at $\pm 30^\circ$, achieved through switching between the two input feed ports of the hybrid coupler.

1. INTRODUCTION

The Industrial, Scientific, and Medical (ISM) bands are a group of frequency bands reserved internationally for the use of radio frequency for industrial, scientific, and medical purposes other than telecommunications. Indeed, there are several ISM bands. However, the most popular one is the band laying between 2.4 GHz and 2.5 GHz due to its freely accessible frequency bands. In addition, around these frequencies there are several applications such as wireless medical devices, Wi-Fi, Wi-Max, Bluetooth, Global Positioning System (GPS), and Radio Frequency Identification (RFID) [1]. These applications cannot function without an antenna, as it plays a crucial role in enabling communication by transforming electrical signals into electromagnetic waves. For these applications, a microstrip antenna is used thanks to its advantages such as: light weight, compact size, low cost, low power consumption, easy manufacturing and integration with modern electronics [2]. Yet, this

antenna type often faces some limitations such as narrow bandwidth, low gain, low directivity, low efficiency, and inflexibility (It radiates energy in a single direction). Indeed, numerous single microstrip elements have been proposed in the literature [3–10], typically characterized by low gain, low directivity, and narrow bandwidth i.e., in [3–10], authors documented low gain between 1.95 and 6 dB and a narrow bandwidth between 4 MHz and 110 MHz (see the table comparison in Section 5). To address the challenge of low gain and narrow bandwidth, researchers have recently investigated a range of microstrip array configurations. Many two-element array configurations have been introduced and extensively discussed in [11–15], i.e., the maximum gain of 9.65 dB was obtained by the authors in [11], and the maximum 10 dB bandwidth of 140 MHz was achieved by the authors in [13]. In addition, various antenna array structures with four-element configurations have been comprehensively analyzed in [16–19] to further enhance gain, i.e., a maximum gain of 13.2 dB is reported by the authors in [17], and the maximum 10 dB bandwidth of 110 MHz was attained by the au-

* Corresponding authors: Ahmed Jamal Abdullah Al-Gburi (ahmedjamal@ieec.org); Abdelaaziz El Ansari (abdelaaziz.elansari1@usmba.ac.ma).

thors in [18]. Moreover, to increase gain more, array antennas structures with eight-elements have been proposed in [20, 21], i.e., the highest gain of 14.64 dB is reached by authors in [20], and the maximum bandwidth of 74 MHz is achieved by authors in [21].

In fact, thanks to the use of array antenna configurations, authors in [11–21] have increased the gain to 14.64 dB. However, they were unable to resolve the issue of narrow bandwidth (with a maximum bandwidth of approximately 140 MHz) and the lack of flexibility in the radiation pattern, due to the use of a T-power splitter to feed the antenna array. To address the challenge of narrow bandwidth and the lack of flexibility, authors in [22–24] replaced the T-power splitter with a directional hybrid coupler as the feed system for the antenna array. In [22], the authors reached the impedance bandwidth of 841 MHz with a peak gain of 8.88 dB and radiation pattern agility. Also, in [23], the authors increase the impedance bandwidth to 902 MHz and the gain to 10.8 dB with radiation pattern agility. These advancements underscore the ongoing efforts to improve antenna performance through innovative feeding mechanisms.

At the same time, Multiple Input Multiple Output (MIMO) technology has emerged as a cornerstone of modern wireless communications, addressing the growing demand for higher data throughput and spectral efficiency. By leveraging multiple transmitting and receiving antennas, MIMO enhances system performance by enabling simultaneous signal streams, reducing interference, and extending coverage. This multi-antenna configuration is particularly valuable in high-density and complex environments. As a foundational technology for 5G and upcoming 6G networks, MIMO supports critical applications such as the Internet of Things (IoT) and vehicular communications, which require high reliability, low latency, and increased capacity [13–14, 16, 25, 26]. Furthermore, to integrate MIMO and advanced antenna designs into compact communication systems, researchers are increasingly focusing on miniaturization techniques. These techniques, including fractal designs, metamaterials, slotted structures, and defected ground planes, address the challenge of reducing antenna size without compromising performance [10].

Hence, in this paper, instead of employing a straight quarter-wave impedance transformer [3–24], which results in a large antenna size, to feed the basic element antenna, we are going to show a new miniaturization method implementing a bent quarter-wave impedance matching device. The miniaturized basic element is used to miniaturize a two-element array antenna which is typically characterized by its narrowband operation and no flexibility. To achieve a wideband directional flexible phased array MIMO antenna, a 3 dB directional coupler is used to feed two identical miniaturized 1×2 array antennas. The innovative approach involves leveraging unique properties of the 3 dB directional coupler, which distributes the input power evenly between its output ports while introducing a precise 90° phase difference. This phase shift is crucial in enabling the array antenna to generate two distinct radiation beams. The dual-beam and MIMO operation is achieved by strategically switching between the input ports of the coupler, allowing the antenna to radiate in two different directions based

on the selected input. The proposed dual-beam antenna prototype has been designed and fabricated on a substrate Rogers RT/duroid 5880 with the following parameters: relative permittivity $\epsilon_r = 2.2$, dielectric loss tangent 0.0009, and total size of $240 \times 136 \times 1.56 \text{ mm}^3$. The simulation results are validated by measurements which confirm that the suggested dual-beam antenna has a high gain of 11.2 dB, a good adaptation, an enhanced bandwidth of 1.22 GHz, and two beams in two different directions $\pm 30^\circ$.

Following this introduction, the article is organized as follows. Section 2 addresses the design of the miniaturized basic element antenna. Section 3 covers the miniaturized 1×2 array antenna. Section 4 presents the design and fabrication of the proposed dual-beam phased array antenna. Section 5 presents comparative analysis of the proposed work and related studies. Finally, the conclusion is summarized in the last section.

2. MINIATURIZED BASIC ELEMENT ANTENNA DESIGN

In compact communication systems, antennas often need to be miniaturized to fit within space constraints while maintaining performance. This need has prompted extensive research into various miniaturization techniques, including fractal designs, metamaterials, slotted configurations, and defected ground plane structures. In this study, we introduce a novel miniaturization approach that employs a bent quarter-wave impedance transformer instead of the traditional straight quarter-wave design [2–17]. The proposed radiating element underwent four optimization steps, with the final step utilizing a curved microstrip line to further reduce the overall size. This method resulted in a 50% size reduction compared to conventional techniques, making the compact element suitable for integration into larger array configurations, such as 1×2 , 1×4 , or even 1×8 arrays, allowing for versatile applications in advanced antenna systems. Each optimization step leading to this miniaturized design is depicted in Figure 1.

The reflection coefficients for each antenna design case are illustrated in Figure 2(a). Case 1 shows the mismatch that occurs when a rectangular antenna is directly connected to a 50Ω transmission line, resulting in significant reflection. In Case 2, the introduction of a quarter-wave impedance transformer reduces the reflection coefficient to below -10 dB; however, the resonance does not align with the target operating frequency. Case 3 adjusts the transformer lengths L_{qw} and L_{50} in an attempt to bring the resonance closer to the desired frequency, but the alignment remains inadequate. Finally, Case 4 incorporates a bent $\lambda/4$ transformer, achieving precise resonance at the target frequency while also reducing the antenna's size. The enhanced resonance at the operating frequency in this final design is clearly demonstrated in Figure 2.

The performance of the proposed miniaturized antenna in terms of reflection coefficient S_{11} , gain, and directivity is shown in Figures 2(a) and (b). This performance has been compared with several previously published works as shown in Table 1. Therefore, the designed basic antenna element has the smallest size of $50 \times 52 \text{ mm}^2$, narrow bandwidth of 26 MHz, and a good gain of 7.11 dB. In the next section, in order to in-

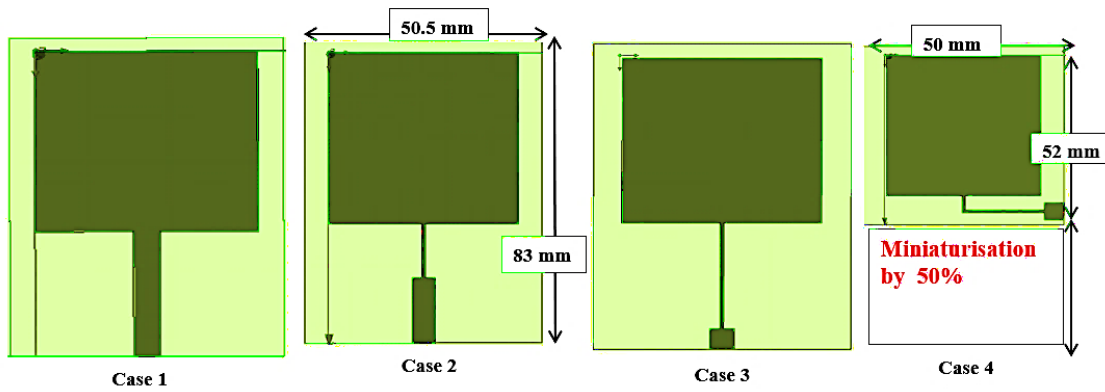


FIGURE 1. Optimization steps of the miniaturized basic element.

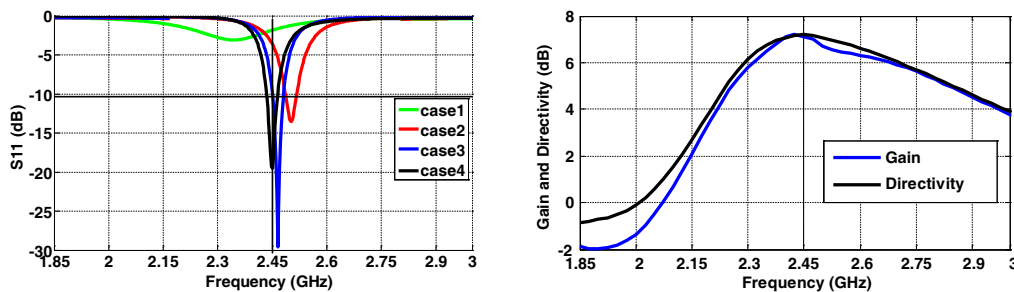


FIGURE 2. Performance of the proposed miniaturized antenna in terms of reflection coefficient, Gain and Directivity.

TABLE 1. Performance comparison of the compact antenna with previous works.

Works. Year	Antenna size (cm ²)	Operational Frequency (GHz)	10-dB bandwidth (MHz)	Peak Directivity (dB)
[3]. 2015	10 × 12	1.75	4	4.2
[4]. 2017	12.3 × 6	2.4	50	6
[5]. 2017	10 × 9	2.4	50	4
[7]. 2018	12.5 × 8.4	2.4	50	4
[9]. 2021	9 × 6.5	2.4	110	4
[11]. 2019	82.8 × 60	2.45	22	7.21
[12]. 2019	83 × 50.5	2.4	24	6.3
[17]. 2020	83 × 50.5	2.4	20	6.32
[19]. 2020	90 × 65	2.4–2.5	32	5
This work	50 × 52	2.45	26	7.11

crease the gain, this miniaturized element will be used to design a compact array antenna of two elements.

3. THE MINIATURIZED 1 × 2 ARRAY ANTENNA

3.1. The T-Magic Power Splitter Used

The hybrid T-junction power splitter presented here is a microwave circuit composed of three T-branch transmission lines, as illustrated in Figure 3. It can function either as a power divider or a power combiner. In this design, the T-junction is used as a 3 dB power divider, where it splits the input power into two equal, in-phase output signals.

The most well-known power divider is 1 × 2 T-shaped power divider. It consists of three T-shaped transmission lines as shown in Figure 3.

To achieve a lossless T-junction, the impedances Z_0 , Z_1 , and Z_2 must satisfy the following equation:

$$\frac{1}{Z_0} = \frac{1}{Z_1} + \frac{1}{Z_2} \tag{1}$$

In microstrip technology, designing a power divider requires considering Equations (1) and (2). These equations enable the conversion between the characteristic impedance and the width of each branch line.

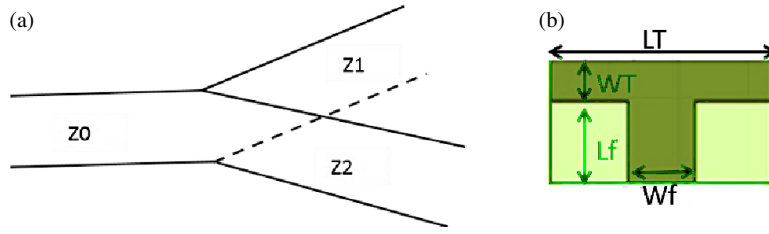


FIGURE 3. (a) 1×2 T-shaped power divider port layout, (b) Design of proposed T power divider.

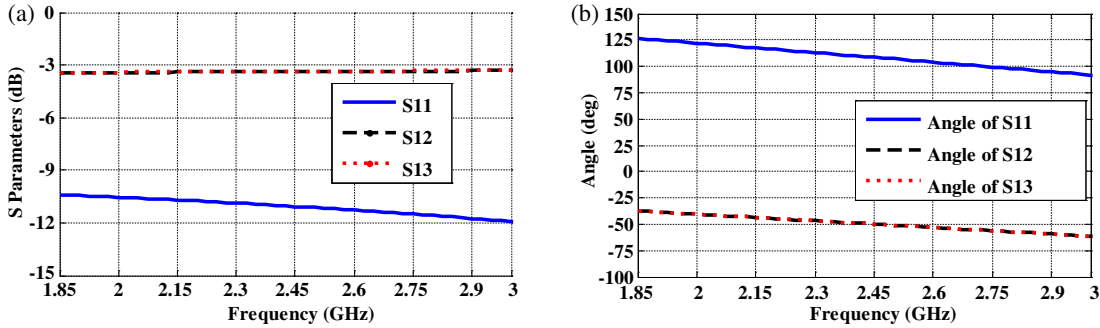


FIGURE 4. Scattering parameters S_{11} , S_{12} , and S_{13} : (a) magnitude as a function of frequency, and (b) plane in degrees as a function of frequency.

The most commonly used feed line in microstrip technology is the one with a characteristic impedance of 50Ω .

Equation (2) allows for the determination of the characteristic impedance Z_{50} based on its width W_{50} :

$$Z_{50} = \frac{120\pi}{\sqrt{\epsilon_r} \left(\frac{W_{50}}{h} + 1.393 + 0.0667 \ln \left(\frac{W_{50}}{h} + 1.44 \right) \right)}$$

$$= < \frac{126}{\sqrt{\epsilon_r}} \quad \text{with } W_{50} > h \quad (2)$$

In contrast, Equation (3) can be utilized to determine the width W_{50} when the impedance Z_{50} is known Z_{50} [1, 27]:

$$\frac{W_{50}}{h} = \frac{2}{\pi} \left[B - 1 - \ln(2B - 1) + \frac{\epsilon_r - 1}{2\epsilon_r} \left(\ln(B - 1) + 0.39 - \frac{0.61}{\epsilon_r} \right) \right] \quad (3)$$

With: $B = \frac{377\pi}{2Z_{50}\sqrt{\epsilon_r}}$, $\frac{W_{50}}{h} > 2$, h the thickness of the substrate, and ϵ_r its relative primitiveness. Z_{50} and W_{50} represent impedance and width, respectively, when the line has a characteristic impedance of 50 Ohm .

In the proposed microstrip T-network power splitter, shown in Figure 3(b), the input impedance is $Z_0 = 50 \Omega$, with a transmission line of length L_f and width W_f . The output arms, each with an impedance of $Z_1 = Z_2 = 100 \Omega$, have respective lengths L_T and widths W_T . This T-junction configuration is optimized to ensure that power is split with minimal loss, achieving balanced signal distribution. The equations that relate the impedance of each T-junction arm to its corresponding width are Equations (2) and (3), detailed above.

A parametric study was conducted on the lengths L_f and L_T to achieve the desired scattering parameters of $S_{12} = S_{13} = -3 \text{ dB}$, with output signals in phase. The optimized parameters for the T-junction power divider are $W_T = 2.78 \text{ mm}$, $W_f = 4.48 \text{ mm}$, $L_T = 16.11 \text{ mm}$, and $L_f = 5.4 \text{ mm}$. Simulation results, presented in Figure 4, illustrate the scattering parameters S_{11} , S_{12} , and S_{13} as functions of frequency. Figure 4(a) shows the magnitudes, while Figure 4(b) displays the phase characteristics. At the target frequency of 2.45 GHz , the reflection coefficient is $S_{11} = -11 \text{ dB}$, and the transmission coefficients S_{12} and S_{13} are both -3.36 dB , indicating balanced signal splitting. The phases of S_{12} and S_{13} are approximately -49.86° and -49.88° , respectively, confirming phase alignment across the frequency range.

3.2. Design of the Miniaturized 1×2 Antenna Array

The suggested miniaturized antenna array is shown in Figure 5. It is made up of two identical miniaturized elements powered by a T-shaped network power splitter. The dimensions of the suggested array antenna are as follow: $L_s = 66 \text{ mm}$, $W_s = 120 \text{ mm}$, $L_p = 39.4 \text{ mm}$, $W_p = 39.3 \text{ mm}$, $L_{qw1} = 21.13 \text{ mm}$, $L_{qw2} = 4 \text{ mm}$, $W_{qw} = 0.74 \text{ mm}$, $L_f = 5.4 \text{ mm}$, $W_f = 4.5 \text{ mm}$, $L_T = 2.8 \text{ mm}$, $W_T = 16.1 \text{ mm}$.

The simulation results of the proposed miniaturized antenna array, generated using the HFSS electromagnetic simulator, are displayed in Figure 6. Figure 6(a) shows the reflection coefficient S_{11} , which measures approximately -27.17 dB at the operating frequency, along with a narrow bandwidth of 52 MHz . In Figure 6(b), the directivity and gain as functions of frequency are presented, revealing a close alignment between the two, with a peak gain of 9.41 dB and a peak directivity of 9.48 dB at 2.45 GHz . Figure 6(c) illustrates the radiation efficiency across the frequency spectrum, achieving a maximum value of 98.16%

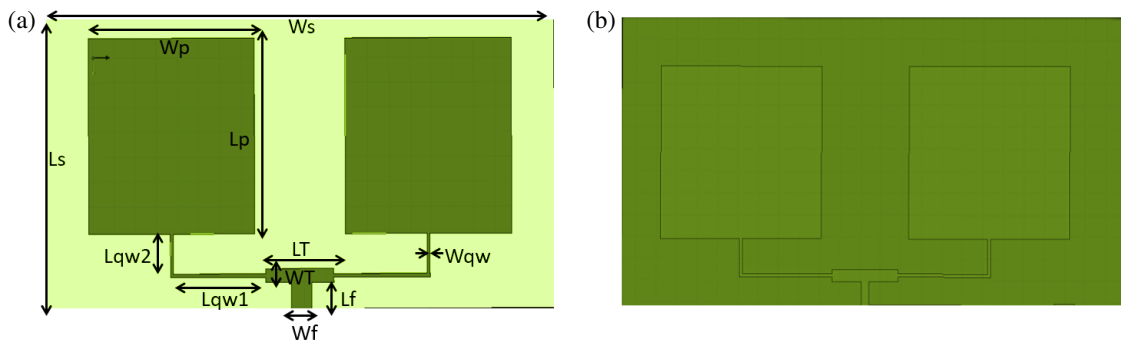


FIGURE 5. Design of the suggested miniaturized antenna array; (a) front view, (b) back view.

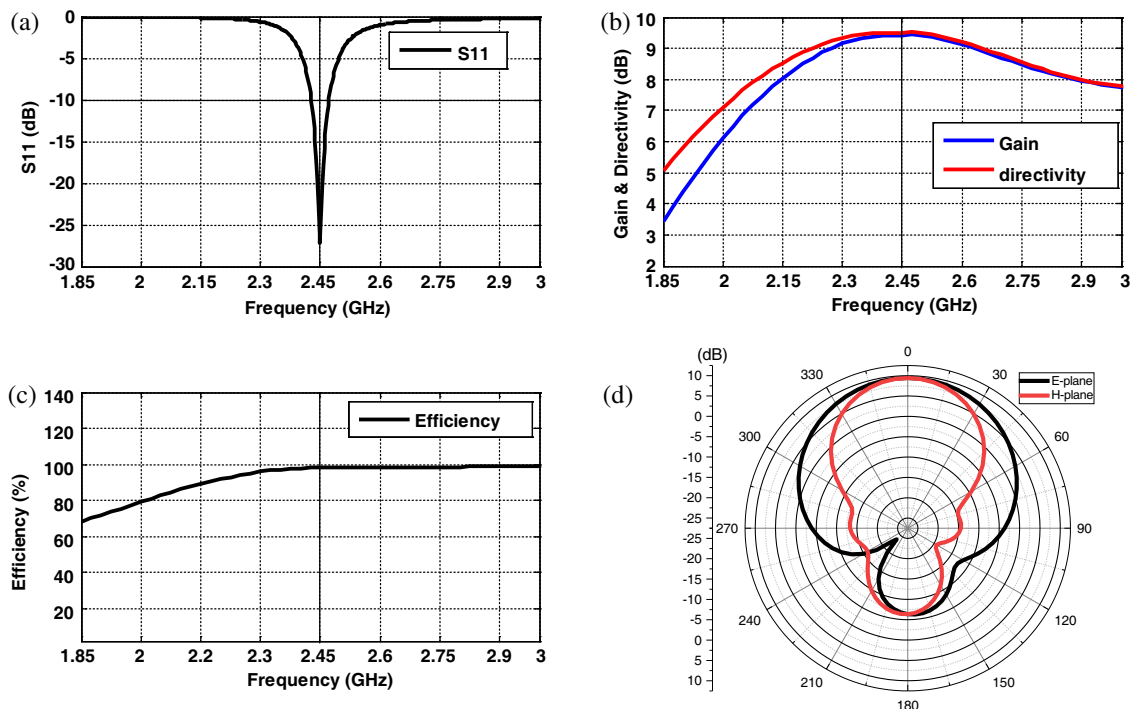


FIGURE 6. (a) Reflection coefficient (S_{11}), (b) Gain and Directivity, (c) Radiation Efficiency, (d) Radiation Patterns in the H and E planes.

at the operating frequency. Finally, Figure 6(d) displays the radiation patterns in both the H and E planes at the operating frequency, demonstrating directional radiation patterns oriented perpendicular to the array antenna plane.

The performance of the proposed miniaturized 1×2 array antenna has been compared with several previously published works in the ISM band around 2.4 GHz, as shown in Table 2. This comparison demonstrates that the presented array antenna is the most compact design while achieving high radiation efficiency and gain. These attributes emphasize its potential for applications where size constraints are critical, further validating the effectiveness of the design methodology used in this study.

To broaden the narrow bandwidth, improve gain, directivity, and radiation coverage, a 3 dB hybrid coupler will be utilized in the next section to feed two identical miniaturized 1×2 array antennas. This will result in a wideband, directional, dual-beam phased 1×4 array antenna.

4. DESIGN AND FABRICATION OF THE PROPOSED DUAL-BEAM PHASED ARRAY ANTENNA

4.1. The Directional Hybrid Coupler 90° Used

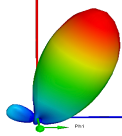
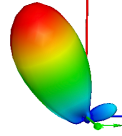
A hybrid coupler is a quadrupole reciprocal microwave circuit that includes two input ports and two output ports. Among the different types available, the 3 dB hybrid coupler is the most widely used, as it effectively splits the input power into two equal portions at its output ports while maintaining a 90-degree phase difference between them.

The microstrip hybrid coupler designed by High Frequency Structure Simulator (HFSS) software is shown in Figure 7. Numerical calculations using the previous Equations (2) and (3) lead to the determination of the width of the parallel and series lines of the coupler using MATLAB software [28]. The proper application of these equations is essential for achieving the desired performance of the coupler in this design.

TABLE 2. Performance comparison of the proposed compact 1×2 array antenna with previous works.

Work. Year	Array configuration	Substrate	Antenna size (cm ²)	Operational Frequency (GHz)	10-dB bandwidth (MHz)	Peak Gain (dB)
[11]. 2019	1×2	Rogers TR5880	11.4×13.5	2.45	34	9.65
[12]. 2020	1×2	Rogers TR5880	8.3×11.05	2.40	54	9.22
[13]. 2019	1×2	Rogers TR5880	10.4×6	2.45	140	5.8
[14]. 2023	1×2	Rogers TR5880	33×5	2.4	22	2.65
[15]. 2023	1×2	Rogers TR5880	19×19	2.4	12	5.54
[16]. 2020	1×2	Rogers TR5880	31.6×31.6	2.4	85	7
This work	1×2	Rogers TR5880	6.6×12	2.45	52	9.42

TABLE 3. Summary of simulated versus measured results of proposed switched directional antenna.

Scenarios	Results	Impedance Bandwidth	Minimum S_{11} value	Minimum VSWR value	Peak Directivity	3D Maximum Beam Direction
When Port 1 is fed	Simulated	1.25 GHz: from 1.725 to 2.96 GHz	-38 dB	1.023	11.54 dB	
	Measured		-44 dB	1.22	11.38 dB	
When Port 2 is fed	Simulated	1.25 GHz: from 1.725 to 2.96 GHz	-15 dB	1.48	11.46 dB	
	Measured		-17 dB	1.38	11.36 dB	

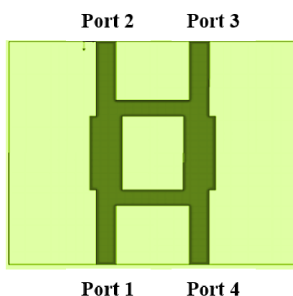


FIGURE 7. Design of the proposed 3 dB directional hybrid coupler.

The designed coupler has a source impedance of $Z_{50} = 50 \Omega$ at their shunt arm and impedance, $\frac{Z_{50}}{\sqrt{2}} = 35.35 \Omega$ at the series arm. The length of each arm is an odd multiple of quarter-wavelength at the operating frequency [17].

$$L = (2k + 1) \frac{\lambda_g}{4} \quad (4)$$

At the operating frequency $F_r = 2.45$ GHz, the first odd multiple is $L_{qw} = \frac{\lambda_g}{4} = 24.13$ mm.

The simulation results for the designed hybrid coupler are shown in Figure 8, which focuses on scattering parameters.

Figure 8(a) displays the magnitude of the scattering parameters in dB as a function of frequency. Notably, the reflection coefficient S_{11} demonstrates a wide bandwidth of 900 MHz, while the isolation S_{14} extends to 1000 MHz. At the resonance frequency of 2.45 GHz, the output signals are measured at approximately -3 dB, indicating that the input energy is effectively divided between the two output ports. In Figure 8(b), the phase angles of the output signals S_{12} and S_{13} are plotted against frequency. This graph reveals a consistent phase shift of approximately 90° between the output signals, which remains stable regardless of whether the input power is applied to port 1 or port 3. This behavior confirms the effective operation of the hybrid coupler as a power divider.

4.2. The Proposed Dual-Beam Phased Array Antenna

Patch antennas are the most frequently used antenna in wireless communication because of their strengths: low cost, low profile, lightness, and smooth integration with PCB (printed circuit board). However, patch antenna suffers from some disadvantages, such as narrow bandwidth, low gain, low directivity, and no flexibility to adapt to smart systems. In this section, we are going to challenge all these disadvantages of the patch antenna.

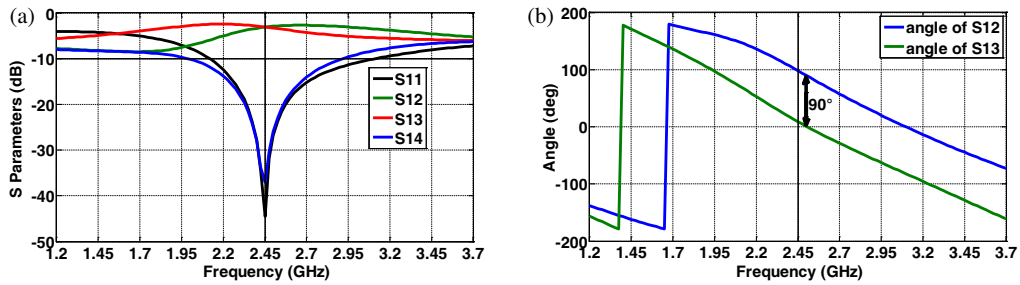


FIGURE 8. Performance of the proposed microstrip hybrid coupler (a) Magnitude in dB of the scattering parameters as a function of frequency, (b) Phase angle in degrees of S_{12} and S_{13} as a function of frequency.

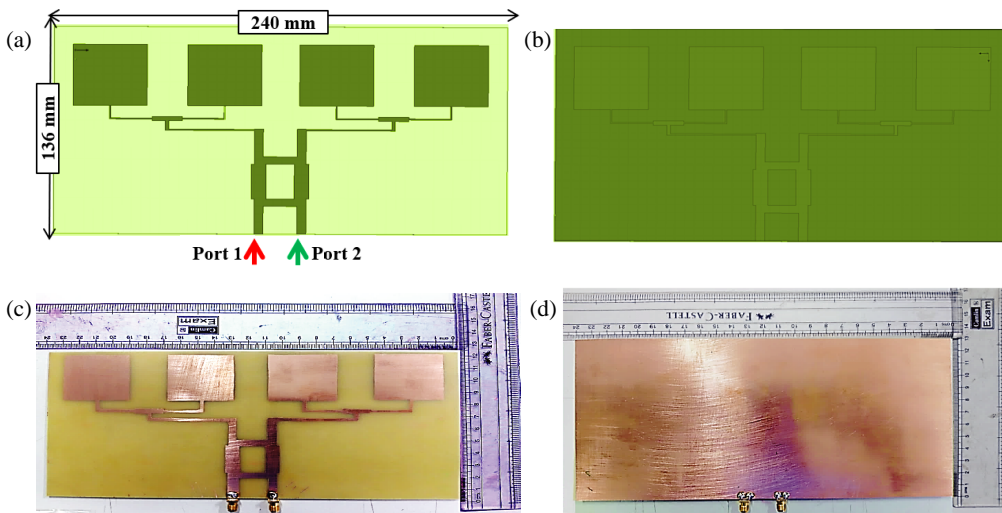


FIGURE 9. Design and fabricated prototype of the proposed 3 dB hybrid coupler feeding 1×4 array antenna, (a) and (b), front view, (c) and (d), back view.

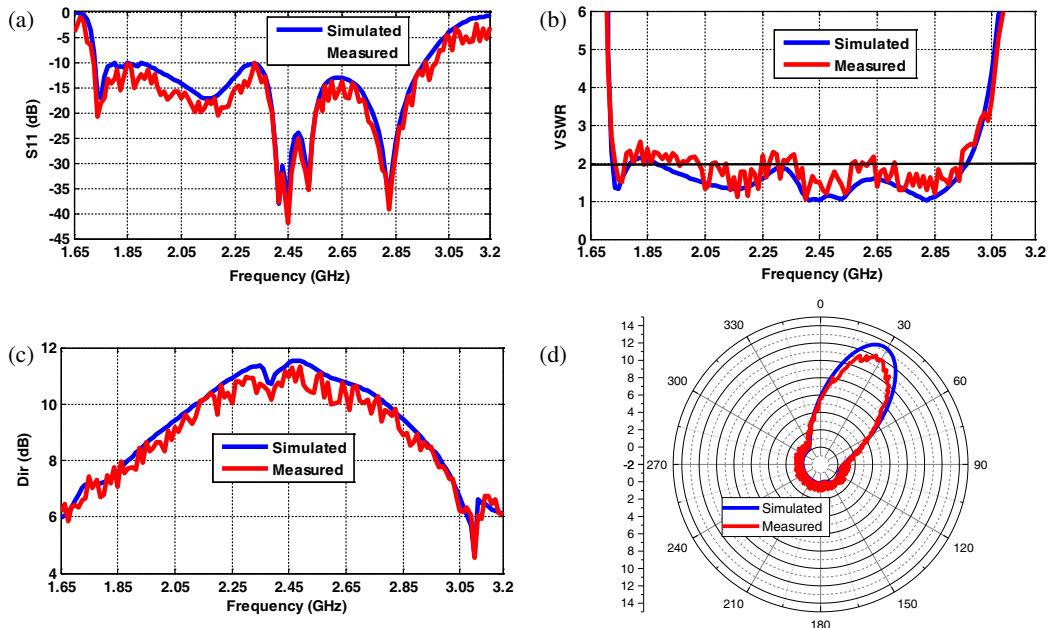


FIGURE 10. Simulation and measurement data for the suggested antenna when input port 1 is powered, (a) S_{11} , (b) VSWR, (c) Directivity, (d) Maximum beam direction in 2D radiation pattern.

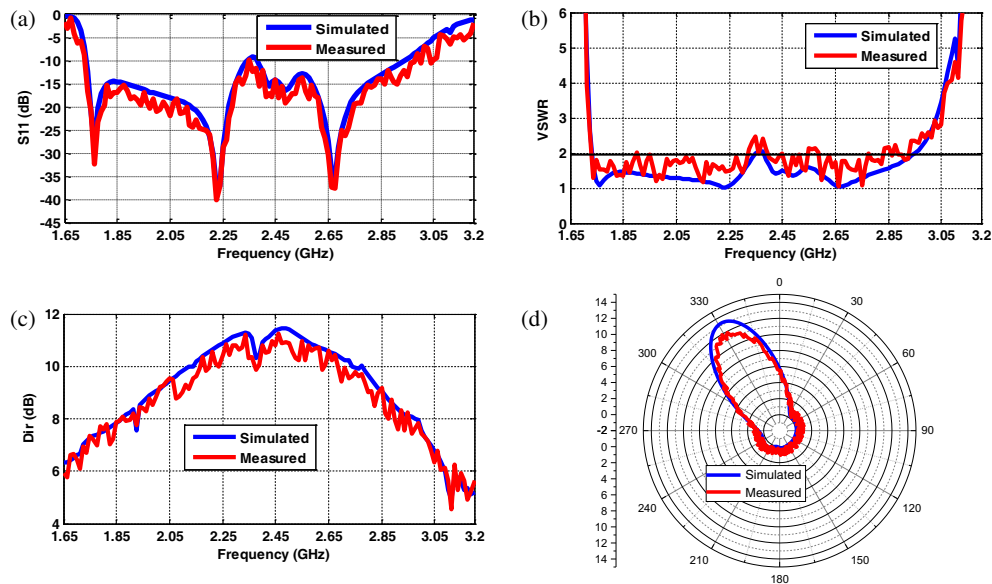


FIGURE 11. Simulation and measurement data for the suggested antenna when input port 2 is powered, (a) S_{11} , (b) VSWR, (c) Directivity, (d) Maximum beam direction in 2D radiation pattern.

TABLE 4. Performance comparison of the proposed dual-beam array antenna with previous works.

Work. Year	Antenna size (cm ²)	Operational Frequency (GHz)	10-dB bandwidth (GHz)	Peak Directivity (dB)	Radiation Pattern Agility	MIMO Capability	Applications
[3]. 2015	10 × 12	1.75	0.004	4.2	No	No	RFID
[4]. 2017	12.3 × 6	2.4	0.050	6	No	No	WLAN full-duplex
[5]. 2017	10 × 9	2.4	0.050	4	No	No	Full-Duplex Communication
[6]. 2018	5 × 5	2.45	0.090	5	No	No	full-duplex devices
[7]. 2018	12.5 × 8.4	2.4	0.050	4	No	No	Full Duplex Transceiver
[8]. 2018	5.1 × 4	2.45	0.042	1.95	No	No	RFID Systems
[9]. 2021	9 × 6.5	2.4	0.110	4	No	No	ISM band
[10]. 2023	5.44 × 4.18	2.45	0.103	2.33	No	No	WLAN
[11]. 2019	11.4 × 13.5	2.45	0.034	9.65	No	No	RFID reader
[12]. 2020	8.3 × 11.05	2.40	0.054	9.22	No	No	RFID reader
[13]. 2019	10.4 × 6	2.45	0.140	5.8	No	Yes	WLAN
[14]. 2023	33 × 5	2.4	0.022	2.65	No	Yes	WLAN
[15]. 2023	19 × 19	2.4	0.012	5.54	No	No	WLAN
[16]. 2020	31.6 × 31.6	2.4	0.085	7	No	Yes	WLAN
[17]. 2019	9.8 × 22.39	2.45	0.056	13.2	No	No	RFID reader
[18]. 2020	22.7 × 9.51	2.45	0.102	7.79	No	No	RFID reader
[19]. 2018	9.1 × 16.1	2.45	0.066	6.63	No	No	RFID reader
[20]. 2022	10.7 × 47.5	2.45	0.062	14.68	No	No	RFID reader
[21]. 2024	11.7 × 47.5	2.45	0.074	14.21	No	No	RFID reader
[22]. 2022	11 × 11.2	2.45	0.841	8.88	Yes	No	RFID reader
This work	13.6 × 24	2.45	1.25	11.22	Yes	Yes	ISM devices

Indeed, the hybrid coupler that we have designed is used to feed two identical 1×2 array antennas. The impedance matching between the patches and coupler is ensured by a folded quarter wave impedance transformer. The proposed dual-beam an-

tenna prototype has been designed and fabricated on a substrate Rogers RT/duroid 5880 with the following parameters: relative permittivity $\epsilon_r = 2.2$, dielectric loss tangent equal 0.0009, and total size of $240 \times 136 \times 1.56 \text{ mm}^3$ as shown in Figure 9.

The simulation results are validated through experimental measurements, as shown in Figures 10 and 11, which illustrate two scenarios: one with port 1 fed and the other with port 4 fed. The antenna's dual-beam functionality is achieved by switching the input power between the two ports of the hybrid coupler. The results demonstrate a significant improvement in performance metrics, including reflection coefficient S_{11} , Voltage Standing Wave Ratio (VSWR), effectively addressing the previously encountered issue of narrow bandwidth. The achieved bandwidth is approximately 1.24 GHz, ranging from 1.72 GHz to 2.95 GHz, as illustrated in Figures 10(a), (b) and 11(a), (b). Figures 10(c) and 11(c) display the directivity versus frequency, and in both scenarios, the peak directivity is approximately 11.52 dB from simulations and 11.36 dB from measurements. This improvement overcomes past limitations of low directivity and gain, resulting in higher directivity and gain in both cases. Figures 10(d) and 11(d) depict the maximum beam direction for each scenario: when port 1 is powered, the beam is directed to the left at -30° , while powering port 4 directs the maximum beam to the right at 30° . Thus, the proposed antenna demonstrates dual-beam capabilities, enhancing operational flexibility. Overall, the proposed antenna is capable of radiating in two distinct directions, coupled with a wide frequency range and high directivity. Table 3 shows a recap of the simulated and measured results of the proposed switched dual-beam directional antenna.

Table 2 provides a detailed summary of the obtained simulated results compared to the measured results. This comparison shows how accurate and reliable the simulation and measurement are.

5. COMPARATIVE ANALYSIS OF THE PROPOSED WORK AND RELATED STUDIES

The performance of the suggested wideband directional dual-beam phased array antenna based on a hybrid coupler has been assessed and contrasted with other studies, as shown in Table 4. According to the data, the suggested dual-beam antenna demonstrates the broadest bandwidth and the greatest directivity that leads to superior gain. Additionally, its beam-switching capability ensures extensive radiation coverage.

6. CONCLUSION

In conclusion, the proposed antenna represents a significant innovation in ISM band applications for the following reasons: its adjustable radiation pattern for enhanced flexibility, dual-beam capability with high gain and directivity, enhanced diversity and multiplexing capabilities, wide impedance bandwidth for extended coverage, and low-cost, low-profile design. These features, together, provide substantial improvements over conventional antenna technologies. Specifically, the adjustable radiation pattern allows for dual beams directed at $\pm 30^\circ$ through input port switching, eliminating the need for physical rotation. This capability enhances reception and signal flexibility in diverse environments. Additionally, the dual-beam configuration ensures better coverage and signal reception, while the high gain and directivity further optimize performance. The an-

tenna's enhanced diversity and multiplexing capabilities, characteristic of MIMO technology, support high data rates and reliable communication. The wide impedance bandwidth ensures efficient operation across the ISM band, and its compact, low-cost design makes it ideal for practical applications with space and budget constraints. The validation of these claims through both simulation and prototype measurements confirms the antenna's potential to meet the demands of modern ISM band communication systems.

ACKNOWLEDGEMENT

The authors wish to express their profound gratitude to Universiti Teknikal Malaysia Melaka (UTeM) and the Malaysian Ministry of Higher Education (MOHE) for their generous support. This work was made possible through the grant PJP/2024/FTKEK/PERINTIS/S01388. The authors would also like to extend their gratitude to Sidi Mohamed Ben Abdellah University, Morocco, for supporting this project.

REFERENCES

- [1] Das, R., T. K. Das, A. K. Yadav, H. C. Mohanta, A. K. M. Z. Hossain, and A. J. A. Al-Gburi, "Analysis of inscribed hexagonal slot loaded antenna for short range RFID reader applications," *Progress In Electromagnetics Research C*, Vol. 150, 125–133, 2024.
- [2] El Arrouch, T., N. E. A. E. Idrissi, and A. E. Ansari, "Microstrip patch antenna using a parasitic mushroom for 5G application at 28 GHz," in *2022 9th International Conference on Wireless Networks and Mobile Communications (WINCOM)*, 1–6, Rabat, Morocco, 2022.
- [3] Turalchuk, P., I. Munina, M. Derkach, O. Vendik, and I. Vendik, "Electrically small loop antennas for RFID applications," *IEEE Antennas and Wireless Propagation Letters*, Vol. 14, 1786–1789, 2015.
- [4] Makar, G., D. Kim, N. Tran, and T. Karacolak, "Compact antennas with reduced self interference for simultaneous transmit and receive," *Progress In Electromagnetics Research C*, Vol. 78, 19–31, 2017.
- [5] Nawaz, H. and I. Tekin, "Dual-polarized, differential fed microstrip patch antennas with very high interport isolation for full-duplex communication," *IEEE Transactions on Antennas and Propagation*, Vol. 65, No. 12, 7355–7360, 2017.
- [6] Goodbody, C., T. Karacolak, and N. Tran, "Dual-polarised patch antenna for in-band full-duplex applications," *Electronics Letters*, Vol. 54, No. 22, 1255–1256, 2018.
- [7] Nawaz, H. and I. Tekin, "Double-differential-fed, dual-polarized patch antenna with 90 dB interport RF isolation for a 2.4 GHz in-band full-duplex transceiver," *IEEE Antennas and Wireless Propagation Letters*, Vol. 17, No. 2, 287–290, 2018.
- [8] Bendali, A., S. Bri, A. E. Fellahi, M. Habibi, and M. N. Srifi, "Printed H-antenna with parasitic element for RFID systems," in *2018 International Symposium on Advanced Electrical and Communication Technologies (ISAECT)*, 1–5, Rabat, Morocco, 2018.
- [9] Lu, K., T. Nguyen, N. Tran, and T. Karacolak, "Parasitic spirals for enhancing bandwidth of a simultaneous transmit and receive patch antenna," *Microsystem Technologies*, Vol. 27, 3333–3338, 2021.

- [10] Laabadli, A., Y. Mejdoub, A. E. Amri, and M. Tarbouch, "Miniaturized metamaterial antenna for 2.45 GHz services," *International Journal of Microwave and Optical Technology*, Vol. 18, No. 4, 349–358, 2023.
- [11] Tabakh, I., M. Jorio, and N. E. A. E. Idrissi, "1 × 2 RFID reader array antenna for narrowband indoor positioning applications," *Journal of Engineering Science and Technology Review*, Vol. 12, No. 6, 167–172, 2019.
- [12] El Alami, A., Y. Ghazaoui, S. Das, S. D. Bennani, and M. E. Ghzaoui, "Design and simulation of RFID array antenna 2 × 1 for detection system of objects or living things in motion," *Procedia Computer Science*, Vol. 151, 1010–1015, 2019.
- [13] Tran, H. H., N. Hussain, and T. T. Le, "Low-profile wideband circularly polarized MIMO antenna with polarization diversity for WLAN applications," *AEU — International Journal of Electronics and Communications*, Vol. 108, 172–180, 2019.
- [14] Sim, C.-Y.-D., V. Dhasarathan, T. K. Tran, J. Kulkarni, B. A. Garner, and Y. Li, "Mutual coupling reduction in dual-band MIMO antenna using parasitic dollar-shaped structure for modern wireless communication," *IEEE Access*, Vol. 11, 5617–5628, 2023.
- [15] Weng, Z., D. Yang, and K. Xue, "Design of a compact microstrip decoupled array," *Electronics*, Vol. 12, No. 19, 4163, 2023.
- [16] Zhang, E., A. Michel, M. R. Pino, P. Nepa, and J. Qiu, "A dual circularly polarized patch antenna with high isolation for MIMO WLAN applications," *IEEE Access*, Vol. 8, 117 833–117 840, 2020.
- [17] El Alami, A., S. Das, B. T. P. Madhav, and S. D. Bennani, "Design, optimization and realization of high gain RFID array antenna 4 × 1 for detection system of objects in motion," *Journal of Instrumentation*, Vol. 14, No. 05, P05002, 2019.
- [18] Tabakh, I., S. Das, M. Jorio, N. E. A. E. Idrissi, S. Mohapatra, and D. Barad, "Defected ground structure (DGS) incorporated RFID reader antenna array for indoor positioning systems at 2.45 GHz," *International Journal of Microwave and Optical Technology*, Vol. 15, No. 6, 517–524, 2020.
- [19] Bendali, A., A. E. Fellahi, M. N. Srifi, S. Bri, and M. Habibi, "A novel adaptive array antenna for a RFID applications," in *2018 International Symposium on Advanced Electrical and Communication Technologies (ISAECT)*, 1–5, Rabat, Morocco, 2018.
- [20] El Ansari, A., S. Das, N. E. A. E. Idrissi, T. El-Arrouch, and A. Bendali, "Slot incorporated high gain Printed RFID Reader Array antenna for 2.4 GHz ISM band applications," in *E3S Web of Conferences*, Vol. 351, 01056, 2022.
- [21] El Ansari, A., S. Das, T. Islam, S. Asha, N. E. A. E. Idrissi, and B. T. P. Madhav, "A high-gain directional 1 × 8 planar antenna array for 2.4 GHz RFID reader applications," *Journal of Circuits, Systems and Computers*, Vol. 33, No. 12, 2450219, 2024.
- [22] Ansari, A. E., S. Das, I. Tabakh, B. T. P. Madhav, A. Bendali, and N. E. A. E. Idrissi, "Design and realization of a broadband multi-beam 1 × 2 array antenna based on 2 × 2 butler matrix for 2.45 GHz RFID reader applications," *Journal of Circuits, Systems and Computers*, Vol. 31, No. 17, 2250305, 2022.
- [23] El Ansari, A., S. Das, T. El-Arrouch, and N. E. A. E. Idrissi, "A hybrid coupler integrated 1 × 4 printed array antenna with broadband and high performance for beamforming RFID reader," in *2022 9th International Conference on Wireless Networks and Mobile Communications (WINCOM)*, 1–6, Rabat, Morocco, 2022.
- [24] Ansari, A. E., V. Jayaprakasan, K. Duraisamy, S. Das, T. El-Arrouch, and N. E. A. E. Idrissi, "A wideband microstrip 1 × 2 array antenna fed by coupler for beam steering terahertz (THz) band applications," *Journal of Nano- and Electronic Physics*, Vol. 15, No. 3, 03028, 2023.
- [25] Abdullah Al-Gburi, A. J., "5G MIMO antenna: Compact design at 28/38 GHz with metamaterial and SAR analysis for mobile phones," *Przełqd Elektrotechniczny*, Vol. 2024, No. 4, 171, 2024.
- [26] Aggarwal, R., A. Roy, and R. Kumar, "A compact four port MIMO antenna for n261 millimeter wave band applications," *Progress In Electromagnetics Research M*, Vol. 129, 33–41, 2024.
- [27] Pozar, D. M., *Microwave Engineering*, John Wiley & Sons, 2011.
- [28] El Ansari, A., L. Kabouri, and E. Ahouzi, "Random attack on Asymmetric Cryptosystem based on phase-truncated fourier transforms," in *2014 International Conference on Next Generation Networks and Services (NGNS)*, 65–68, Casablanca, Morocco, 2014.